# Measurement of the production of high-mass $\gamma\gamma$, $\pi^0\pi^0$, and $\gamma\pi^0$ pairs in $\pi^- p$, $\pi^+ p$, and $pp$ collisions at 300 GeV/$c$

C. De Marzo, M. De Palma, C. Favuzzi, G. Maggi, E. Nappi, F. Posa, A. Ranieri, G. Selvaggi, and P. Spinelli
*Dipartimento di Fisica dell'Universita di Bari and Istituto Nazionale di Fisica Nucleare, Bari, Italy*

A. Bamberger, M. Fuchs, W. Heck, C. Loos, R. Marx, K. Runge, E. Skodzek, C. Weber, M. Wülker, and F. Zetsche
*University of Freiburg, Freiburg, Germany*

V. Artemiev, Yu. Galaktionov, A. Gordeev, Yu. Gorodkov, Yu. Kamyshkov, V. Plyaskin, V. Pojidaev, V. Shevchenko, E. Shumilov, and V. Tchudakov
*Institute of Theoretical and Experimental Physics, Moscow, U.S.S.R.*

J. Bunn,* J. Fent, P. Freund, J. Gebauer, M. Glas, P. Polakos,† K. Pretzl,‡ T. Schouten,§ P. Seyboth, J. Seyerlein, and G. Vesztergombi**
*Max-Planck-Institut für Physik und Astrophysik, München, Germany*

(NA24 Collaboration)

(Received 14 November 1989)

The NA24 experiment at CERN investigated inclusive $\gamma\gamma$, $\pi^0\pi^0$, and $\gamma\pi^0$ final states in the mass range between 4 and 9 GeV/$c^2$ produced in $\pi^- p$, $\pi^+ p$, and $pp$ reactions at a c.m.-system energy $\sqrt{s}=23.7$ GeV. The $\pi^0\pi^0$ cross sections agree well with expectations of the quark-parton model. For $\gamma\pi^0$ production in $\pi^- p$ and $pp$ reactions, a clear signal is observed and cross sections are shown. The production of $\gamma\gamma$ events was observed with a statistical significance of $2.9\sigma$ in $\pi^- p$ reactions. The cross section is in agreement with a higher-order QCD prediction.

## I. INTRODUCTION

The measurement of direct photon production with high transverse momentum $p_T$ in hadron-hadron collisions has turned out to be a useful tool to test the validity of the quantum-chromodynamical description of parton-parton scattering processes. Direct photons provide a rather clean insight into the hadrons because they couple pointlike to the partons without any subsequent fragmentation.

Here we present the measurement of the production of events containing two direct photons, two $\pi^0$'s plus a direct photon, plus a $\pi^0$ in hadron-hadron collisions (henceforth referred to as $\gamma\gamma$, $\pi^0\pi^0$, and $\gamma\pi^0$ events, respectively). Results on inclusive direct photon and $\pi^0$ production obtained by this experiment are already published.[1,2]

As pointed out in several theoretical papers[3-11] double-photon production provides information about quark charges, intrinsic parton transverse momenta $\kappa_T$, and a QCD process of $O(\alpha^2\alpha_s^2)$ which is described by the so-called box graph and contributes to the cross section considerably at low $x$. Additionally by comparing single- and double-photon production one can determine the strong coupling constant $\alpha_s$.

Experimentally, however, it is very difficult to distinguish between direct photons and photons from the decay of neutral mesons, mainly $\pi^0$'s and $\eta$'s. The mesons are much more copiously produced in the so-far accessible kinematic region. Nevertheless several experiments using various techniques have reported a signal of photon pairs in hadron-hadron reactions.[12-17] This experiment used a fine-grained electromagnetic (em) calorimeter in which the em showers of an event and therefore the $\pi^0$'s and $\eta$'s could be recognized with high efficiency. Because direct photons are quite rarely produced due to their em origin the detector had to be operated in a high-intensity particle beam ($10^7$ particles/s).

After the description of the detector, the selection of the data sample, the event reconstruction, and the determination of the corrections will be discussed. While searching for $\gamma\gamma$ events, $\pi^0\pi^0$ and $\gamma\pi^0$ events had to be measured as well. Therefore results on these types of events were also obtained and will be shown additionally.

## II. APPARATUS

The NA24 experiment, which is described in more detail elsewhere,[1] was installed in a secondary beam of the super proton synchrotron (SPS) at CERN. Beams containing $\pi^-$ or a mixture of $\pi^+$ ($\sim 13\%$) and protons ($\sim 87\%$) with an intensity of typically $10^7$ particles/s and a momentum of 300 GeV/$c$ hit a 1-m-long liquid-hydrogen target. Two CEDAR Čerenkov counters identified the $\pi^+$ and protons of the positive beam. Upstream of the target two iron walls and between them an array of veto scintillation counters were set up to reduce triggers from upstream interactions or muon halo.

The particles originating from an interaction in the hydrogen target traversed several multiwire proportional chambers[18,19] (MWPC's). These contained a total of 22 wire planes. They were used to reconstruct the tracks of charged particles and the event vertex.

The calorimeter system which was positioned at a distance of 8.35 m from the target center consisted of three parts.

(1) The so-called photon position detector[20] (PPD) with a thickness of $9.6X_0$ which measured the position of single em showers with high space resolution. Its four independent quadrants covering an area of $3\times3$ m$^2$ with a central hole of $0.5\times0.5$ m$^2$ consisted of alternating layers of lead ($1.1X_0$) and of proportional tubes with triangular shape oriented horizontally, vertically, and with an inclination of 45°. The distance of two wires in neighboring tubes was 0.773 cm. A pressure regulation system reduced the gas gain variations to $\pm2\%$.

(2) The ring calorimeter[21,22] which measured the energy not contained in the PPD. It was subdivided laterally into 240 read-out cells. Longitudinally it was divided into an em section ($16X_0$, lead/scintillator sandwich) and a hadronic section ($6\lambda_a$, iron/scintillator sandwich) which were read out separately.

(3) The downstream calorimeter[22] which measured the energy flow through the 56-cm diameter hole of the ring calorimeter.

The calorimeters were calibrated with electron and hadron beams of known energies between 5 and 170 GeV. For em showers the combined system of the PPD and the em section of the ring calorimeter had an energy resolution of $0.28/\sqrt{E\ (\mathrm{GeV})}$ and a nonuniformity of $\pm2\%$ as determined by beam scans across the detector. The fine-tuning of the calibration was performed with the $\pi^0$ mass peak. A check of this calibration with the $\eta$ mass peak yielded a discrepancy of 1% which was assumed to be the systematic error of the absolute energy scale.

The trigger selected events with high-$p_T$ em clusters. Its logical structure was subdivided into several levels of more and more stringent trigger conditions. A trigger reduction of 1 event in $10^5$ interactions with a dead time of only 20% at a beam intensity of typically $10^7$ particles per second was achieved. For most of the data the highest trigger level was provided by digital trigger processors (one for each PPD quadrant) by which it was possible to select simultaneously events containing one em cluster with $p_T > 3.75$ GeV/$c$ ($1\gamma$ trigger) or two em clusters in two different PPD quadrants with $p_T > 2$ GeV/$c$ ($2\gamma$ trigger).

## III. DATA SAMPLE AND DATA ANALYSIS

The data taken by the $2\gamma$ trigger made up the main part of the statistics for this analysis. The sensitivities were 1245, 139, and 356 events/nbarn in $\pi^- p$, $\pi^+ p$, and $pp$ reactions, respectively. Additionally a data sample was used which was collected by a $1\gamma$ trigger at a threshold of $p_T > 3.75$ GeV/$c$ before the trigger processors were installed. Thus the sensitivities for events in which one trigger particle carried a transverse momentum greater than 4 GeV/$c$ was enhanced to 1757, 246, and 584 events/nbarn.

The data were treated in the same way as in our earlier reported work.[1,2] Only events with a vertex inside the 70-cm-long fiducial volume of the target were retained. A vertex was defined by the crossing of at least three tracks reconstructed in the MWPC's. Triggers from beam parallel background, caused by upstream interactions or muon halo, were discarded by the following two requirements. (i) The total energy of an event measured in the calorimetric system had to be consistent with the beam energy. This cut also removed background from pile-up in the calorimeters. (ii) The signals of both triggering em showers had to be in time with the interaction in the target. It was not necessary to apply an additional cut on the direction of the em showers because the observation of two coincident em showers itself reduced the remaining beam parallel background to a negligible level.

In the next step em showers in the PPD were reconstructed. Energy clusters found in the PPD projections were combined to showers in space using energy-correlation and shower-development criteria which were determined by calibration data. The energy measured in the em part of the corresponding ring calorimeter cells was added. Then for each trigger quadrant the effective masses of the trigger shower with all other showers were calculated. If such a mass combination was found to lie in the range between 50 and 210 MeV/$c^2$ (470 and 620 MeV/$c^2$) the shower pair was classified as a $\pi^0$ ($\eta$); otherwise the shower was considered a direct photon candidate provided its width was consistent with that of a single photon.

The corrections for the reconstruction efficiency and the energy resolution and the background from misidentified $\pi^0$'s and $\eta$'s were calculated by means of a Monte Carlo (MC) program. This program simulated the detector response of one single photon, $\pi^0$ or $\eta$ per event using the measured signals from calibration showers. We achieved a realistic distribution of the MC-generated events in $p_T$ and rapidity $y$ by weighting them with the parametrization of the measured $\pi^0$ spectrum.[23] The MC events were then reconstructed by the same program as the experimental data. The MC simulation described the experimental data generally very well[1]; a small discrepancy appears in the distribution of the $\pi^0$ decay asymmetry

$$A = \left| \frac{E_1 - E_2}{E_1 + E_2} \right|$$

($E_1$ and $E_2$ being the energies of the two photons) for $A > 0.8$. For the determination of the $\pi^0$ cross sections this region with $A > 0.8$ was discarded. For the estimation of the background in the direct photon candidates this discrepancy was taken into account as part of the systematic error. The resulting single-particle correction and background factors were applied to both particles of the considered final states; this was a good approximation for the two-particle corrections because it can be assumed that the two particles are only weakly correlated in $p_T$ and $y$ and because the correction and background factors were quite insensitive to variations of the slope of the $p_T$ distribution.

As an upper limit for the number of reconstructed $\pi^0$'s in $\pi^0\pi^0$ and $\gamma\pi^0$ events all photon-photon mass combinations in the allowed range with a decay asymmetry $A < 0.8$ were taken. A lower limit was determined by subtracting a fraction of possible combinatorial background which was estimated by comparing mass peaks with and without away-side trigger particle. In the latter case the combinatorial background was negligible. The $\pi^0$ mass peak of the $2\gamma$ trigger data however showed a clear enhancement in its tails. It could not be decided whether this enhancement was caused by a poorer mass resolution due to the not fully sensitive $2\gamma$ trigger (see below) or by an actual combinatorial background. The latter may be larger in two-particle final states because on average there is also an enhancement of the charged-particle multiplicity around a $\pi^0$ with high $p_T$ if another high-$p_T$ particle is observed in the same event (Fig. 1). This uncertainty in the combinatorial background induced a $p_T$-dependent systematic error on the $\pi^0$ rate determination which was however negligible above $p_T > 3.5$ GeV/$c$.

The efficiency of the $2\gamma$ trigger had to be determined experimentally, whereas the efficiency of the $1\gamma$ trigger was 100% at $p_T > 4$ GeV/$c$ as verified by comparing data sets with different thresholds. In estimating the $2\gamma$ trigger efficiency all $1\gamma$ trigger data were used in which the $2\gamma$ trigger was active in parallel. In these events two showers with transverse momenta $p_{T1}$ and $p_{T2}$ had to be reconstructed where $p_{T1} > p_{T2}$ and $p_{T1} > 4$ GeV/$c$ had to be satisfied. The $2\gamma$ trigger efficiency for one trigger particle dependent on $p_{T2}$ was then determined by counting the events in which the $2\gamma$ trigger bit was switched on. As shown in Fig. 2 the $2\gamma$ trigger had quite a broad turn on region caused by a nonlinearity of the flash analog-to-digital converters which measured the shower energies for the trigger processors. A correction for the trigger efficiency, as parametrized by the curves shown in Fig. 2, was applied to the data.

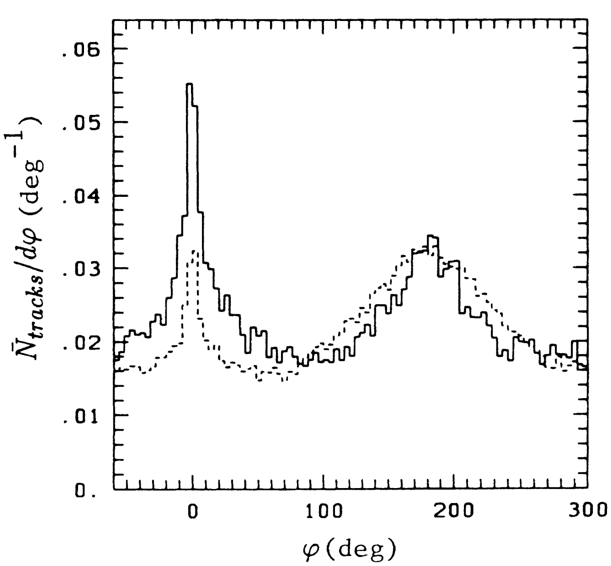


FIG. 1. Average number $\bar{N}_{\text{tracks}}$ of charged particles per event and per degree vs the azimuthal angle $\varphi$. The zero of $\varphi$ is defined by a $\pi^0$ with a transverse momentum between 2 and 3 GeV/$c$. The solid histogram is the distribution for events in which a second $\pi^0$ was observed with a transverse momentum in the same range. For the dashed histogram the observation of an additional $\pi^0$ was not required.

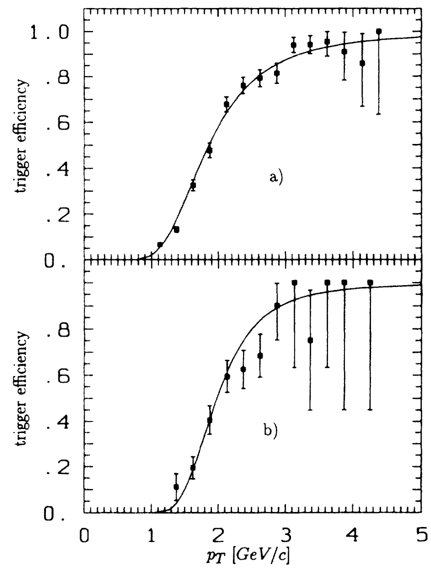


FIG. 2. Efficiency of the $2\gamma$ trigger vs the transverse momentum $p_T$ of one trigger particle in (a) for $\pi^- p$, in (b) for $\pi^+ p$ and $pp$ reactions. The curves show a function of the form $1/[1+1/a(p_T-b)^c]$ which was fitted to the data points.

In order to eliminate edge effects in the calorimeters the geometrical acceptance was restricted to a c.m.-system (c.m.s.) rapidity from $-0.65$ to $+0.52$. Also strips of a width of 16 cm, centered at the adjacent edges of the PPD quadrants, were excluded. Because of the trigger logic the trigger particles had to lie in two different quadrants. Therefore the azimuthal difference of the two trigger particles was larger than a minimum value which lay between 7.8° and 34.2° depending on the distance of the shower impact points from the beam axis.

## IV. RESULTS

In this section we present our results on inclusive $\pi^0\pi^0$, $\gamma\pi^0$, and $\gamma\gamma$ production. When quoting the measurement errors the following conventions are chosen. The statistical uncertainty for numerical values (e.g., in tables) is quoted as the first error. The second error represents the systematic uncertainty in the combinatorial background and/or the background of misidentified mesons in the direct photon candidate sample. In the figures the statistical error is drawn as a vertical bar at the data points, whereas the range of the quadratic sum of statisti-

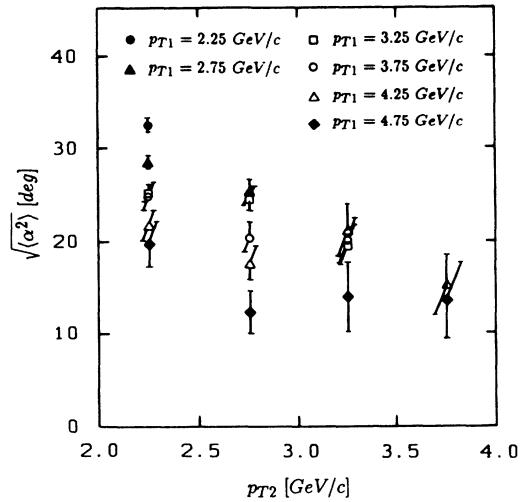


FIG. 3. Width $\langle \alpha^2 \rangle^{1/2}$ of the distributions of the azimuthal correlation angle $\alpha$ for various $\pi^0$ transverse momenta $p_{T1}$ and $p_{T2}$ in $\pi^- p$ reactions. The angle $\alpha$ is defined as $\alpha = 180° - \alpha$, where $\varphi$ stands for the azimuthal angle difference of the $\pi^0$'s.

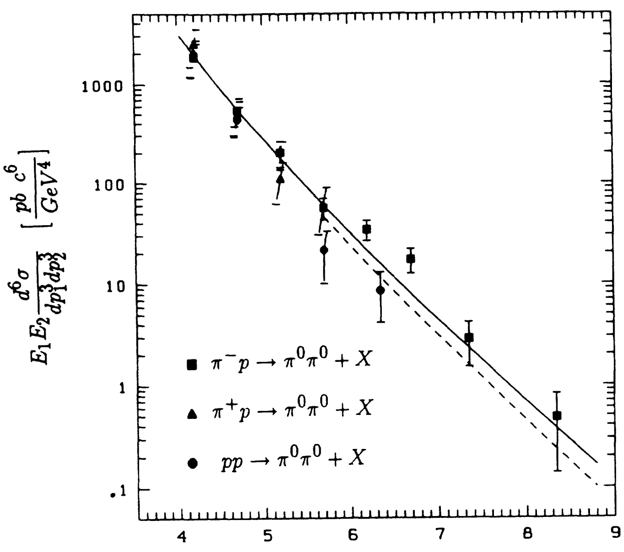


FIG. 4. Invariant double-differential cross section for inclusive $\pi^0\pi^0$ production in $\pi^- p$, $\pi^+ p$, and $pp$ reactions vs the sum $M' = p_{T1} + p_{T2}$ of the $\pi^0$ transverse momenta. The curves show a function of the form $F(x_T, M') = A(1-x_T)^b (M'/2)^k$ which was fitted to the measured cross section of the reaction $p\text{Be} \to \pi^-\pi^+ + X$ in Ref. 28 for $x_T > 0.17$ (solid line) and $x_T > 0.24$ (dashed line), where $x_T = M'/\sqrt{s}$. For comparison the curves were scaled down by a factor of 18 as explained in the text.

cal and systematic errors is indicated by short horizontal lines. An additional global normalization error on the events rates which was estimated to be $\pm 10\%$ and the uncertainty in the transverse-momentum scale of $\pm 1\%$ are not shown in the tables and figures.

### A. Inclusive $\pi^0\pi^0$ production

The two $\pi^0$'s have a clear tendency to be produced with opposite transverse momenta, i.e., with an azimuthal difference $\varphi$ of 180°. Deviations from this are characterized by an angle $\alpha$, defined as $\alpha = 180° - \varphi$. Figure 3 shows that the r.m.s. deviation $\langle \alpha^2 \rangle^{1/2}$ of $\alpha$ distributions decreases with increasing transverse momenta $p_{T1}$ and $p_{T2}$ of both $\pi^0$'s. At high transverse momenta however $\langle \alpha^2 \rangle^{1/2}$ seems to reach a minimum value of about 13°. This effect was already observed in a CERN ISR experiment.[24] The angular correlation of the two $\pi^0$'s and the azimuthal distribution of the tracks of charged particles (see Fig. 1) shows that the event structure is mainly two-jet like. This indicates that essentially hard $2 \to 2$ parton scattering processes already underlie the production of the two high-$p_T$ $\pi^0$'s at this relatively low c.m.s. energy. Selecting events at the same c.m.s. energy by a global transverse energy trigger did not result in events with dominant jet structure[25] in contrast with the situation at the highest ISR energies (see, e.g., Ref. 26) or at the CERN S$p\bar{p}$S collider (see, e.g., Ref. 27).

The invariant double-differential cross section for $\pi^0\pi^0$ production versus $M' = p_{T1} + p_{T2}$ is shown in Fig. 4 and Table I. One may compare it with a measurement of the

TABLE I. Invariant double-differential cross sections for inclusive $\pi^0\pi^0$ production in $\pi^- p$, $\pi^+ p$, and $pp$ reactions at $\sqrt{s} = 23.7$ GeV vs $M' = p_{T1} + p_{T2}$, where $p_{T1}$ and $p_{T2}$ are the transverse momenta of the $\pi^0$'s. The cross sections are averaged over the transverse-momentum difference $P'_T = p_{T1} - p_{T2}$ up to a value of $P'^{\max}_T$, which is listed in the second column.

| | | $E_1 E_2 \frac{d^6\sigma}{dp_1^3 dp_2^3}$ (pb $c^6$/GeV$^4$) | | |
|---|---|---|---|---|
| $M'$ (GeV/$c$) | $\lvert P'^{\max}_T \rvert$(GeV/$c$) | $\pi^- p$ | $\pi^+ p$ | $pp$ |
| 4.20 | 0.5 | $(1.83 \pm 0.12 \pm 0.66) \times 10^{+3}$ | $(2.49 \pm 0.44 \pm 0.92) \times 10^{+3}$ | $(1.94 \pm 0.25 \pm 0.71) \times 10^{+3}$ |
| 4.70 | 0.75 | $(5.53 \pm 0.43 \pm 1.68) \times 10^{+2}$ | $(4.91 \pm 1.18 \pm 1.44) \times 10^{+2}$ | $(4.45 \pm 0.76 \pm 1.32) \times 10^{+2}$ |
| 5.20 | 1.10 | $(2.03 \pm 0.33 \pm 0.49) \times 10^{+2}$ | $(4.91 \pm 1.18 \pm 1.44) \times 10^{+2}$ | $(1.11 \pm 0.42 \pm 0.26) \times 10^{+2}$ |
| 5.70 | 1.10 | $(5.76 \pm 0.90 \pm 1.03) \times 10^{+1}$ | $(6.06 \pm 2.81 \pm 1.01) \times 10^{+1}$ | $(2.18 \pm 1.09 \pm 0.40) \times 10^{+1}$ |
| 6.20 | 1.10 | $(3.43 \pm 0.64 \pm 0.41) \times 10^{+1}$ | | |
| 6.35 | 1.10 | | | $(8.57 \pm 4.29 \pm 1.00) \times 10^{+0}$ |
| 6.70 | 1.10 | $(1.74 \pm 0.46 \pm 0.12) \times 10^{+1}$ | | |
| 7.35 | 1.10 | $(2.85 \pm 1.34 \pm 0.0) \times 10^{+0}$ | | |
| 8.35 | 1.10 | $(4.81 \pm 3.41 \pm 0.0) \times 10^{-1}$ | | |

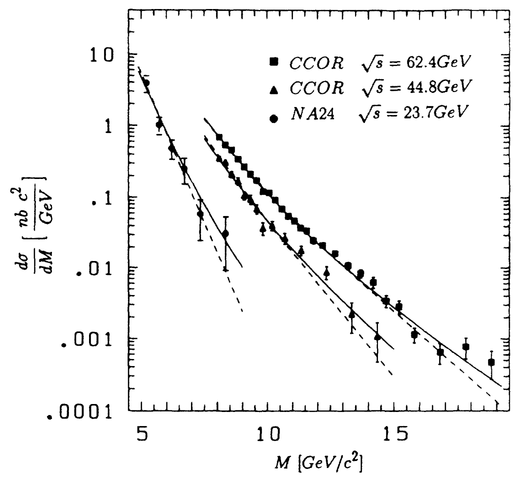


FIG. 5. Cross section $d\sigma/dM$ for inclusive $\pi^0\pi^0$ production in $pp$ reactions as defined in Eq. (4.1) of the text. The scaling functions $(d\sigma/dM)_1 = A_1 M^{-n_1} e^{-b_1 x}$ (solid line) and $(d\sigma/dM)_2 = A_2 M^{-n_2} e^{-b_2 x^2}$ (dashed line) were fitted to the measurements at the c.m.s. energies $\sqrt{s} = 62.4$ GeV and $\sqrt{s} = 44.8$ GeV in Ref. 29 and were extrapolated to the NA24 c.m.s. energy $\sqrt{s} = 23.7$ GeV.

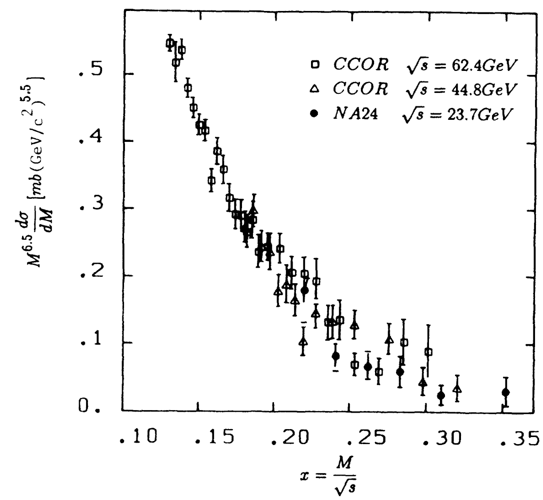


FIG. 6. The scaled cross section $M^{6.5} d\sigma/dM$ ($M$ in units of GeV/$c^2$) for inclusive $\pi^0\pi^0$ production in $pp$ reactions. The agreement of the scaled cross-section measurements at the various c.m.s. energies demonstrates the validity of the scaling hypothesis of Ref. 29.

reaction $pBe \rightarrow \pi^+\pi^- + X$ at 300 GeV in a Fermilab experiment.[28] In order to have comparable acceptances the c.m.s. rapidity $y$ of each $\pi^0$ was restricted to $-0.17$ to $+0.5$ and the angle $\alpha$ was restricted to be less than 7.1°. The Fermilab cross section is scaled by a factor $\frac{1}{18}$ to take into account the mass number $A$ of Be ($A = 9$) and the combinatorial factor of $\frac{1}{2}$ for the comparison of $\pi^0\pi^0$ with $\pi^+\pi^-$ production. The absolute value of $P'_T = p_{T1} - p_{T2}$ was restricted to be less than $P'^{\max}_T = 1.1$ GeV/$c$ as in the Fermilab experiment. Only in bins with low $M'$ was a more stringent $P'_T$ cut applied (see Table I) to avoid $p_T$ regions where the corrections are no longer reliable. At low values of $M'$ the experiments show good agreement within statistical and systematic errors. For $\pi^- p$ reactions however the measured cross section at large $M'$ lies systematically above the Fermilab curves. This can be explained in the framework of the parton model, since the probability to find a parton carrying a large fraction of the total momentum of the hadron is higher in $\pi$ mesons than in protons.

A test of a scaling hypothesis which was carried out by the CERN-Columbia-Oxford-Rockefeller (CCOR) Collaboration in $pp$ reactions at the CERN Intersecting Storage Rings[29] was extended to the NA24 c.m.s. energy of $\sqrt{s} = 23.7$ GeV. The cross section measured by the CCOR collaboration was [see Eq. (1) of Ref. 29]:

$$\frac{d\sigma}{dM} = \frac{1}{0.7}\int_{-0.35}^{+0.35} dY \int_{-0.4}^{+0.4} d\cos\theta^* \int_0^1 dP_T \left[\frac{d^4\sigma}{dM\,dY\,dP_T d\cos\theta^*}\right]. \tag{4.1}$$

According to the geometrical acceptance of the CCOR experiment the maximal angle $\alpha$ was 40°. In Eq. (4.1) $M$ is the invariant mass, $P_T = |\mathbf{p}_{T1} + \mathbf{p}_{T2}|$ the absolute value of the net transverse momentum, and $Y$ the c.m.s. rapidity of the $\pi^0$ pair. The quantity $\cos\theta^* = \frac{1}{2}(\theta_1^* + \theta_2^*)$ is the mean cosine of the polar angles $\theta_1^*$ and $\theta_2^*$ of the $\pi^0$'s measured in a system where the $\pi^0$ pair momentum along the beam axis vanishes. This system approximately coincides with the parton c.m.s. system. To correct for the geometrical acceptance with respect to the pair rapidity $Y$ our cross section is multiplied by a global correction factor of 1.16 as determined by a MC program. The program calculated $\pi^0$ pair production in $pp$ reactions according to QCD in the approximation of the leading logarithms.[30] Figure 5 shows the resulting cross section of this experiment (see also Table II) compared with those of CCOR. The two scaling functions

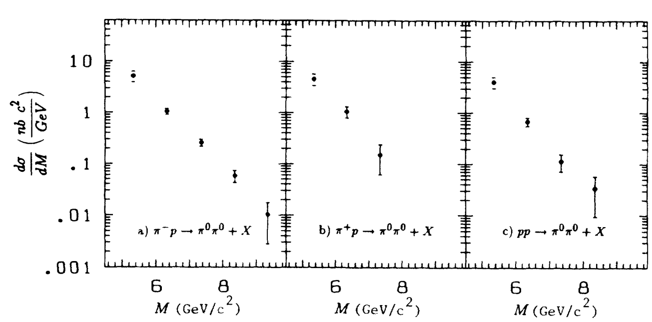


FIG. 7. Cross section $d\sigma/dM$ for inclusive $\pi^0\pi^0$ production in (a) $\pi^- p$, (b) $\pi^+ p$, and (c) $pp$ reactions vs the $\pi^0$ pair mass $M$. The cross section is integrated over the full geometrical acceptance of the NA24 detector. The maximum accepted difference of the transverse momenta of the $\pi^0$'s was 1 GeV/$c$.

TABLE II. Cross section $d\sigma/dM$ for inclusive $\pi^0\pi^0$ production in $pp$ reactions as defined in Eq. (4.1) in dependence of the invariant $\pi^0$ pair mass $M$ at $\sqrt{s}=23.7$ GeV.

| $M$ [GeV/$c^2$] | $\frac{d\sigma}{dM}$ (nb $c^2$/GeV) |
|---|---|
| 5.21 | $(3.94\pm0.40\pm0.96)\times10^{0}$ |
| 5.71 | $(1.01\pm0.20\pm0.19)\times10^{0}$ |
| 6.21 | $(4.80\pm1.27\pm0.62)\times10^{-1}$ |
| 6.71 | $(2.51\pm0.96\pm0.23)\times10^{-1}$ |
| 7.34 | $(5.87\pm3.40\pm0.33)\times10^{-2}$ |
| 8.34 | $(3.13\pm2.22\pm0.00)\times10^{-2}$ |

$$\left[\frac{d\sigma}{dM}\right]_1 = A_1 M^{-n_1} e^{-b_1 x},$$
$$\left[\frac{d\sigma}{dM}\right]_2 = A_2 M^{-n_2} e^{-b_2 x^2}, \tag{4.2}$$

where $x=M/\sqrt{s}$, are shown by the solid and dashed curves, respectively. The parameters were fitted by the CCOR experiment and had the values

$$A_1=28.1\times10^{-28}\ \text{cm}^2,\quad n_1=6.40,\quad b_1=14.2\ ,$$
$$A_2=11.6\times10^{-28}\ \text{cm}^2,\quad n_2=6.55,\quad b_2=38.9\ . \tag{4.3}$$

In Fig. 6 the cross sections are scaled by a factor $M^{6.5}$ and the scaled values seem to agree at the different c.m.s. energies. From Figs. 5 and 6 one can conclude that the scaling hypothesis is valid down to the NA24 c.m.s. energy in an $x$ range from approximately 0.2 to 0.4.

Figure 7 and Table III show the inclusive $\pi^0\pi^0$ cross section $d\sigma/dM$ with $|P_T'|<1$ GeV/$c$ integrated over the total geometrical acceptance of our detector. The cross-section ratio

$$\frac{d\sigma}{dM}(\pi^- p\to\pi^0\pi^0+X)\Big/\frac{d\sigma}{dM}(pp\to\pi^0\pi^0+X)$$

rises with both $M$ and $Y$ [Figs. 8(a), 9(a), and 9(b)], whereas the ratio

$$\frac{d\sigma}{dM}(\pi^- p\to\pi^0\pi^0+X)\Big/\frac{d\sigma}{dM}(\pi^+ p\to\pi^0\pi^0+X)$$

is statistically compatible with 1 [Figs. 8(b), 9(c), and 9(d)]. This is again a consequence of the fact that the parton distribution functions in $\pi$ mesons are harder than those in protons. Fixing the transverse momentum of the first $\pi^0$ one observes a strong decrease of the cross section with increasing $\zeta=p_{T2}/p_{T1}$ (Fig. 10). This is caused by the steep decrease of the fragmentation functions with the increase of the fraction of the parton momentum carried by the $\pi^0$.

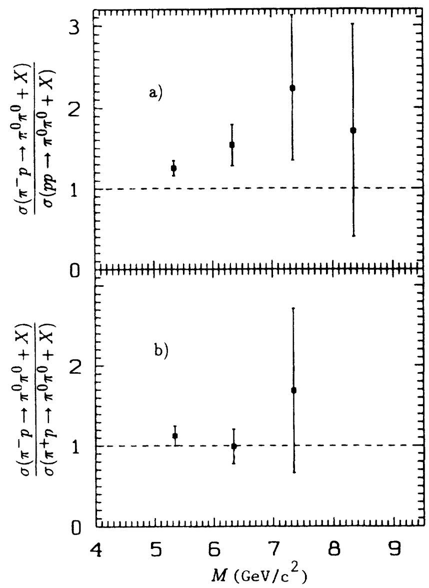


FIG. 8. Cross-section ratios for inclusive $\pi^0\pi^0$ production in $\pi^- p$ and $pp$ reactions (a) and in $\pi^- p$ and $\pi^+ p$ reactions (b) vs the invariant $\pi^0$ pair mass $M$. The kinematic region is as for Fig. 7.

### B. Inclusive $\gamma\pi^0$ production

Because of the trigger bias and the uncertainty in the combinatorial background to the $\pi^0$'s a statistically significant signal of $\gamma\pi^0$ events was only obtained if an isolation cut was applied to the photon candidates, so that they were essentially not accompanied by other particles. A trigger particle was considered to be isolated, if the following conditions were satisfied.

(1) *Cluster cut.* In the PPD quadrant with a $\pi^0$ or $\eta$ only two clusters with an energy greater than $E_{\text{cl}}^{\max}>1.5$ GeV were reconstructed. For photon candidates only one such cluster was allowed.

(2) *Tracks cut.* The PPD impact point of all charged

TABLE III. Cross section $d\sigma/dM$ for inclusive $\pi^0\pi^0$ production in $\pi^- p$, $\pi^+ p$, and $pp$ reactions in dependence of the invariant $\pi^0$ pair mass $M$, integrated over the total geometrical acceptance of the NA24 detector. The maximum accepted difference of the transverse momenta $p_{T1}$ and $p_{T2}$ of the $\pi^0$'s was 1 GeV/$c$.

| | | $\frac{d\sigma}{dM}$ (nb $c^2$/GeV) | |
|---|---|---|---|
| $M$ (GeV/$c^2$) | $\pi^- p$ | $\pi^+ p$ | $pp$ |
| 5.34 | $(5.08\pm0.17\pm1.16)\times10^{+0}$ | $(4.52\pm0.49\pm1.04)\times10^{+0}$ | $(4.07\pm0.27\pm0.95)\times10^{+0}$ |
| 6.34 | $(1.04\pm0.07\pm1.12)\times10^{+0}$ | $(1.05\pm0.22\pm0.13)\times10^{+0}$ | $(6.78\pm1.03\pm0.77)\times10^{-1}$ |
| 7.35 | $(2.55\pm0.38\pm1.00)\times10^{-1}$ | $(1.51\pm0.89\pm0.07)\times10^{-1}$ | $(1.14\pm0.42\pm0.07)\times10^{-1}$ |
| 8.35 | $(5.75\pm1.54\pm1.54)\times10^{-2}$ | | $(3.37\pm2.42\pm2.41)\times10^{-2}$ |
| 9.35 | $(1.02\pm0.74\pm0.74)\times10^{-2}$ | | |

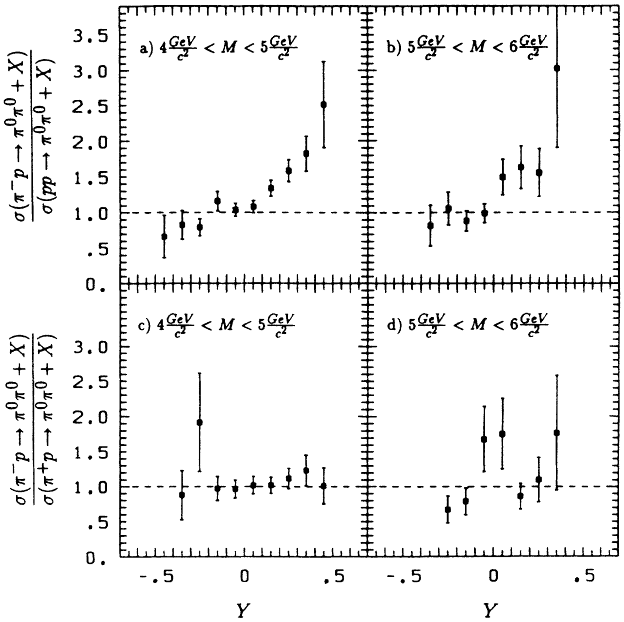


FIG. 9. Cross-section ratios for inclusive $\pi^0\pi^0$ production in $\pi^- p$ and $pp$ reactions (a) and (b) and in $\pi^- p$ and $\pi^+ p$ reactions (c) and (d) vs the $\pi^0$ pair rapidity $Y$ for two different intervals of the $\pi^0$ pair mass $M$.

particles reconstructed in the MWPC system had to have a distance $\rho > 21$ cm from the trigger photon impact point. Tracks hitting the detector less than 1 cm from the photon impact point were disregarded in order not to discard photons which had converted into an $e^+e^-$ pair.

(3) *Hadron energy cut.* The energy in the hadronic section of the ring calorimeter in a $3\times3$ matrix of cells centered on the trigger photon impact point had to be less than $E_h^{\max}$. The value of $E_h^{\max}$ was five times the energy $E_h^{\max 0}$ at which 1% of isolated photons would have been discarded.

From the Monte Carlo simulation it was found that less than 2% of isolated produced photons are removed by the isolation cut when shower fluctuations of big showers are sometimes treated as an additional real shower by the reconstruction program. No restrictions were of course applied to the away side $\pi^0$.

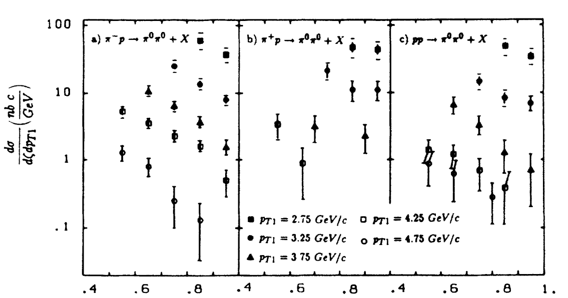


FIG. 10. Inclusive $\pi^0\pi^0$ cross section vs the ratio $\zeta = p_{T2}/p_{T1}$ of the transverse momenta $p_{T1}$ and $p_{T2}$ of the $\pi^0$'s for various values of $p_{T1}$. The transverse momenta are ordered such that $p_{T1} > p_{T2}$.

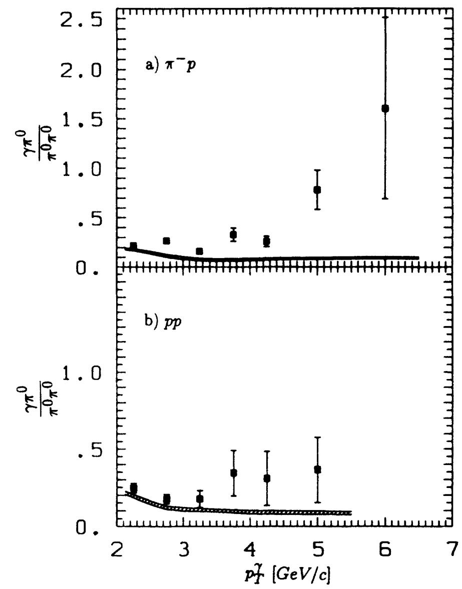


FIG. 11. Ratio $R_{\gamma\pi^0}/R_{\pi^0\pi^0}$ of the uncorrected numbers of events vs the transverse momentum $p_T^\gamma$ of the photon. $R_{\gamma\pi^0}$ is the uncorrected number of $\gamma\pi^0$ candidates and $R_{\pi^0\pi^0}$ is the uncorrected number of $\pi^0\pi^0$ events, in which one of the $\pi^0$'s carries the same transverse momentum as the photon candidate. This $\pi^0$ and the photon candidate had to satisfy the isolations cuts (see text). The transverse momentum of the away side $\pi^0$ had to exceed 2 GeV/$c$. The hatched band shows the MC-estimated background and its systematic uncertainty.

For $\pi^- p$ and $pp$ reactions Fig. 11 shows the ratio of the uncorrected number of $\gamma\pi^0$ candidates in dependence of the transverse momentum $p_T^\gamma$ of the photon candidate divided by the uncorrected number of $\pi^0\pi^0$ events. In the

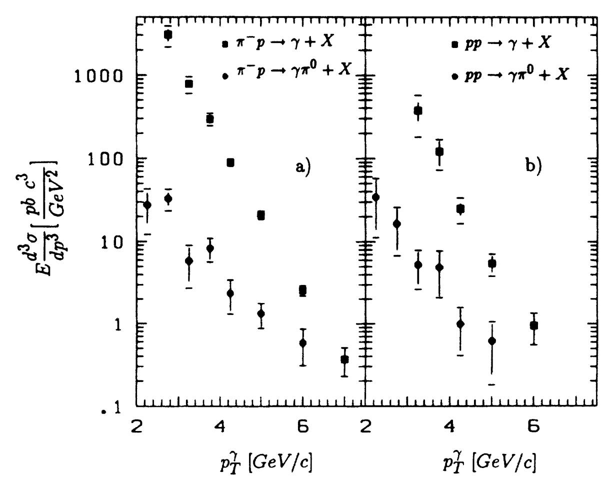


FIG. 12. Invariant cross section of inclusive direct photon production in $\pi^- p$ (a) and $pp$ reactions (b) vs the transverse momentum $p_T^\gamma$ of the photon. The squares show the fully inclusive photon cross section (Ref. 1). The dots show the cross section for $\gamma\pi^0$ events where the photon satisfies the isolation cuts (see text) and the $\pi^0$ carries a transverse momentum larger than 2 GeV/$c$.

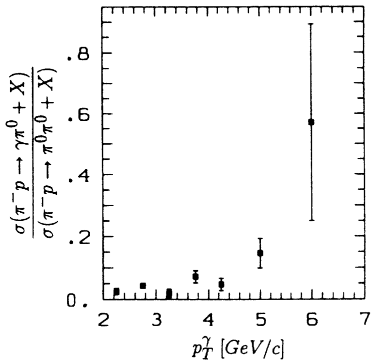


FIG. 13. Ratio of the cross sections for inclusive production of $\gamma\pi^0$ and $\pi^0\pi^0$ events vs the photon transverse momentum $p_T^\gamma$ in $\pi^-p$ collisions. One of the $\pi^0$'s in the $\pi^0\pi^0$ events had to have the same transverse momentum $p_T^\gamma$ as the photon. The transverse momentum of the away-side $\pi^0$ had to exceed 2 GeV/$c$. The photon had to satisfy the isolation criteria (see text).

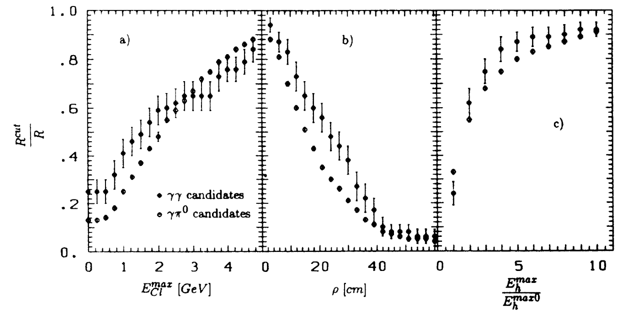


FIG. 14. Ratio of the uncorrected number $R^{\text{cut}}$ of $\gamma\gamma$ and $\gamma\pi^0$ candidates, respectively, which survive the cluster cut (a), the tracks cut (b), and the hadron energy cut (c), and the corresponding total number of candidates $R$. The ratio $R^{\text{cut}}/R$ is plotted vs the corresponding isolation parameter. The transverse momenta of both trigger particles had to exceed 2 GeV/$c$.

$\pi^0\pi^0$ events a $\pi^0$ was randomly selected from the pair and treated like the photon; i.e., it had to satisfy the isolation cuts. The away-side $\pi^0$ had to carry a transverse momentum greater than 2 GeV/$c$. There is a clear excess of $\gamma\pi^0$ events above the MC-estimated background from misidentified $\pi^0\pi^0$ and $\eta\pi^0$ events (hatched band in Fig. 11). The systematic uncertainty in this background which is deduced from the discrepancy between the distributions of the $\pi^0$ decay asymmetry $A$ in the data and the MC simulation corresponds to the width of the hatched band of Fig. 11. Despite the isolation cuts it was not possible to extract a statistically significant signal of $\gamma\pi^0$ events in $\pi^+p$ reactions because the luminosity for this reaction was too low.

The invariant cross section for $\gamma\pi^0$ events in $\pi^-p$ and $pp$ reactions versus the transverse momentum $p_T^\gamma$ of the photon is shown by the dots in Fig. 12 and listed in Table IV. Again the photon had to satisfy the isolation cuts and the transverse momentum $p_T^{\pi^0}$ of the $\pi^0$ had to exceed 2 GeV/$c$. From QCD calculations it was estimated[9] that photons from quark bremsstrahlung, which may be accompanied by other particles, contribute less than 20% to the fully inclusive direct photon cross section. A comparison of $\gamma\pi^0$ production with our fully inclusive direct photon cross sections[1] is shown in Fig. 12. One finds that the $\gamma\pi^0$ cross sections are much lower and show a shallower decrease with $p_T^\gamma$. In $\pi^-p$ reactions the cross-section ratio of $\gamma\pi^0$ and $\pi^0\pi^0$ production shows a clear rise with increasing $p_T^\gamma$ (see Fig. 13).

In most of the $\gamma\pi^0$ events $p_T^\gamma$ is larger than $p_T^{\pi^0}$ (see Table V). This asymmetry is consistent with the expectation that the photons are direct participants in the parton scattering process whereas $\pi^0$'s are fragmentation products and therefore carry only a fraction of the transverse momentum of the partons. Neglecting intrinsic transverse momenta of the partons the events with $p_T^\gamma < p_T^{\pi^0}$ are only produced if the photon is radiated off a quark via bremsstrahlung or if at the parton level a three-body final state is produced.

### C. Inclusive $\gamma\gamma$ production

Because of systematic uncertainties and because of effects of the not fully efficient $2\gamma$ trigger it was not possible to extract a statistically significant signal of $\gamma\gamma$ events by estimating the background from misidentified $\pi^0\pi^0$, $\pi^0\eta$, $\gamma\pi^0$, etc., events directly by the MC simulation of the experiment. Therefore a more indirect method was chosen taking advantage of the QCD prediction that direct photons are produced predominantly isolated whereas $\pi^0$'s and $\eta$'s are often accompanied by other par-

TABLE IV. Invariant cross section for inclusive $\gamma\pi^0$ production in $\pi^-p$ and $pp$ reactions as a function of the photon transverse momentum $p_T^\gamma$. The photon had to satisfy the isolation criteria and the transverse momentum of the $\pi^0$ had to exceed 2 GeV/$c$.

| | $E^\gamma \frac{d^3\sigma}{(dp^\gamma)^3}$ (pb $c^3$/GeV$^2$) | |
|---|---|---|
| $p_T^\gamma$ (GeV/$c$) | $\pi^-p$ | $pp$ |
| 2.25 | $(2.76\pm1.08\pm1.10)\times10^{+1}$ | $(3.42\pm2.03\pm1.08)\times10^{+1}$ |
| 2.75 | $(3.29\pm0.56\pm0.77)\times10^{+1}$ | $(1.64\pm0.84\pm0.46)\times10^{+1}$ |
| 3.25 | $(5.84\pm2.54\pm1.79)\times10^{+0}$ | $(5.30\pm2.19\pm1.48)\times10^{+0}$ |
| 3.75 | $(8.25\pm2.15\pm1.46)\times10^{+0}$ | $(4.95\pm2.74\pm0.81)\times10^{+0}$ |
| 4.25 | $(2.35\pm0.93\pm0.49)\times10^{+0}$ | $(9.94\pm5.22\pm2.63)\times10^{-1}$ |
| 5.00 | $(1.33\pm0.41\pm0.19)\times10^{+0}$ | $(6.19\pm3.78\pm2.32)\times10^{-1}$ |
| 6.00 | $(5.82\pm2.71\pm0.50)\times10^{-1}$ | |

TABLE V. Corrected number of $\gamma\pi^0$ events for various intervals of the transverse momenta $p_T^\gamma$ and $p_T^{\pi^0}$ of the photon and the $\pi^0$, respectively. Again the photon had to satisfy the isolation criteria.

| $p_T^\gamma$(GeV/$c$) \ $p_T^{\pi^0}$(GeV/$c$) | 2.0–2.5 | 2.5–3.0 | 3.0–3.5 | 3.4–4.0 | 4.0–5.5 | >5.5 |
|---|---|---|---|---|---|---|
| 2.0–2.5 | 178.2±95.5±74.1 | 156.4±58.8±31.7 | | | | |
| 2.5–3.0 | 498.0±77.8±118.6 | 109.1±32.5±18.5 | 78.4±23.1±3.7 | | | |
| 3.0–3.5 | | 103.1±29.5±21.5 | 30.6±13.0±2.3 | 9.2±7.4±0.7 | | |
| 3.5–4.0 | | | 50.6±17.4±2.9 | 15.3±10.1±0.6 | 0 | |
| 4.0–5.5 | | | | 33.3±16.0±0.4 | 8.4±7.3±0 | 0 |
| >5.5 | | | | | 4.6±4.6±0.0 | 0 |

ticles. From the total number of $\gamma\gamma$ candidates such events were excluded in which both photons match the impact point of a track of a charged particle within 1 cm. Hence contributions of Drell-Yan pairs to the $\gamma\gamma$ sample are strongly suppressed.

The rates of $\gamma\gamma$ and $\gamma\pi^0$ candidates surviving the isolation cuts of Sec. IV B are shown by Figs. 14(a)–14(c). For a range of cut parameters a larger fraction of $\gamma\gamma$ candidates than of $\gamma\pi^0$ candidates is seen to remain. This is expected if true $\gamma\gamma$ events are among the $\gamma\gamma$ candidates. At extreme values of the cut parameters either all candidates are rejected due to small fluctuations in the calorimeter energy signals [small $E_{\rm Cl}^{\max}$, $E_h^{\max}$ in Figs. 14(a) and 14(c)] or the cuts become ineffective in discriminating the two processes [large $E_{\rm Cl}^{\max}$, $\rho$, $E_h^{\max}$ in Figs. 14(a)–14(c)]. The cut parameters were therefore chosen in the center of the efficient discrimination range. The stability of the procedure was checked by varying the cut parameters in the ranges $1<E_{\rm Cl}^{\max}<3$ GeV, $10<\rho<30$ cm, $3<E_h^{\max}/E_h^{\max 0}<7$. The resulting number of $\gamma\gamma$ events was found to change by less than 5%.

To extract the number of $\gamma\gamma$ events from the difference of event numbers with and without isolation cuts the following definitions were used:

$$X=\frac{R_{\gamma\gamma}^{\rm cut}}{R_{\gamma\gamma}}=\frac{N_{\gamma\gamma}^{\rm cut}+U^{\rm cut}}{N_{\gamma\gamma}+U}\ , \tag{4.4}$$

$$Y=\frac{R_{\gamma\pi^0}^{\rm cut}}{R_{\gamma\pi^0}}\ , \tag{4.5}$$

$$S=\frac{N_{\gamma\gamma}}{U}\ , \tag{4.6}$$

with $R_{\gamma\gamma}$ the number of $\gamma\gamma$ candidates, $R_{\gamma\gamma}^{\rm cut}$ the number of $\gamma\gamma$ candidates with isolation cut, $N_{\gamma\gamma}$ the number of $\gamma\gamma$ events, $N_{\gamma\gamma}^{\rm cut}$ the number of $\gamma\gamma$ events with isolation cut, $R_{\gamma\pi^0}$ the number of $\gamma\pi^0$ candidates, $R_{\gamma\pi^0}^{\rm cut}$ the number of $\gamma\pi^0$ candidates with isolation cut, $U$ the background to $\gamma\gamma$ candidates, and $U^{\rm cut}$ the background to $\gamma\gamma$ candidates with isolation cut.

With $R_{\gamma\gamma}=N_{\gamma\gamma}+U$ and (4.6) one obtains

$$N_{\gamma\gamma}=\frac{S}{S+1}R_{\gamma\gamma}\ . \tag{4.7}$$

Because the $\gamma\pi^0$ candidates are contaminated by misidentified $\pi^0\pi^0$ and $\eta\pi^0$ events it can be shown that they represent the correct mixture of event types which contribute to the background in the $\gamma\gamma$ candidate sample:

$$Y=\frac{R_{\gamma\pi^0}^{\rm cut}}{R_{\gamma\pi^0}}=\frac{U^{\rm cut}}{U}\ . \tag{4.8}$$

With the assumption that a fraction $\epsilon$ of good $\gamma\gamma$ events is retained by the isolation cut, i.e., $N_{\gamma\gamma}^{\rm cut}=\epsilon N_{\gamma\gamma}$, one obtains

$$S=\frac{X-Y}{\epsilon-X}\ . \tag{4.9}$$

Neglecting processes where direct photons are produced accompanied by other particles $\epsilon$ can be assumed to be very close to 1. From the MC simulation it was found that only 2% of isolated produced photons are removed by the isolation cut; therefore $\epsilon$ was set to 0.96.

The measured values of $X$ and $Y$ are listed in Table VI

TABLE VI. Numbers $R_{\gamma\gamma}$ and $R_{\gamma\pi^0}$ of $\gamma\gamma$ and $\gamma\pi^0$ events in which both trigger particles carry a transverse momentum greater than 2 GeV/$c$. The numbers $R_{\gamma\gamma}^{\rm cut}$ and $R_{\gamma\pi^0}^{\rm cut}$ are the corresponding numbers for events where both trigger particles also satisfy the isolation criteria.

| Reaction | $R_{\gamma\gamma}$ | $R_{\gamma\gamma}^{\rm cut}$ | $X=\frac{R_{\gamma\gamma}^{\rm cut}}{R_{\gamma\gamma}}$ | $R_{\gamma\pi^0}$ | $R_{\gamma\pi^0}^{\rm cut}$ | $Y=\frac{R_{\gamma\pi^0}^{\rm cut}}{R_{\gamma\pi^0}}$ |
|---|---|---|---|---|---|---|
| $\pi^- p$ | 67 | 23 | 0.34±0.06 | 1287 | 198 | 0.15±0.01 |
| $\pi^+ p$ | 8 | 2 | 0.25±0.15 | 82 | 13 | 0.16±0.04 |
| $pp$ | 18 | 3 | 0.17±0.09 | 258 | 54 | 0.21±0.03 |

TABLE VII. Invariant cross section for inclusive $\gamma\gamma$ production versus the transverse momentum $p_{T1}^{\gamma}$ of one of the photons. The cross section is integrated over $z=\mathbf{p}_{T1}^{\gamma}\cdot\mathbf{p}_{T2}^{\gamma}/(\mathbf{p}_{T1}^{\gamma})^2$ of the other photon above the listed values $z^{\min}$.

| $p_{T1}^{\gamma}$ (GeV/$c$) | $z^{\min}$ | $E\frac{d^3\sigma}{dp^3}$ (pb $c^2$/GeV$^2$) |
|---|---|---|
| 2.75 | 0.80 | $2.07^{+0.53}_{-0.92}\times10^{0}$ |
| 3.50 | 0.67 | $7.0^{+2.3}_{-3.6}\times10^{-1}$ |
| 4.50 | 0.50 | $9.3^{+13.3}_{-9.3}\times10^{-2}$ |

and determine the value of $S$ to be $0.30\pm0.12$ in $\pi^-p$ reactions. From formula (4.7) one obtains a number $N_{\gamma\gamma}$ of $\gamma\gamma$ events of $15.5^{+4.39}_{-5.29}$ with both photons having a transverse momentum larger than 2 GeV/$c$. The error corresponds to a statistical significance of $2.9\sigma$.

The invariant cross section for inclusive $\gamma\gamma$ production in $\pi^-p$ reactions versus the transverse momentum $p_{T1}^{\gamma}$ of one of the photons is shown in Fig. 15 and listed in Table VII. It was integrated over the variable $z=\mathbf{p}_{T1}^{\gamma}\cdot\mathbf{p}_{T2}^{\gamma}/(\mathbf{p}_{T1}^{\gamma})^2$ of the other photon above a value of $z^{\min}=p_{T2}^{\min}/p_{T1}^{\min}$, where $p_{T1}^{\min}$ is the low edge of the considered bin of the transverse momentum $p_{T1}^{\gamma}$. The minimal transverse momentum $p_{T2}^{\min}$ of the other photon was $p_{T2}^{\min}=2$ GeV/$c$. For each event both photons enter the cross section. From Fig. 15 one can see that the $\gamma\gamma$ cross section agrees within the statistical errors with a perturbative QCD calculation[10] (full line) which takes into account the terms up to $O(\alpha^2\alpha_s)$ and includes also the box process of $O(\alpha^2\alpha_s^2)$. The dashed-dotted line shows the prediction without the bremsstrahlung contribution. The latter amounts to less than 10% of the cross section. The contribution of the Born term is shown by the dashed line. The calculation uses for the QCD scales in the strong coupling constant and in the structure functions the definition $Q^2=(p_{T1}^{\gamma})^2$, a QCD scale parameter $\Lambda=0.2$ GeV and the structure functions of set I of Ref. 31. The result of the calculation[10] is corrected by a factor 0.50 because the theoretical cross section was integrated over the full rapidity range of the second photon whereas the detector measures only in the central rapidity region from $-0.65$ to 0.52. The factor was determined by a MC integration of the Born term of $\gamma\gamma$ production and it was assumed to be approximately valid for the higher-order calculation.

Because of the low luminosities no statistically significant signal of $\gamma\gamma$ events could be extracted for $\pi^+p$ and $pp$ reactions. Therefore upper limits for the cross-section ratios $\sigma(\pi^+p\to\gamma\gamma+X)/\sigma(\pi^-p\to\gamma\gamma+X)$ and $\sigma(pp\to\gamma\gamma+X)/\sigma(\pi^-p\to\gamma\gamma+X)$ are given in Table VIII and are compared with theoretical expectations derived in Ref. 10.

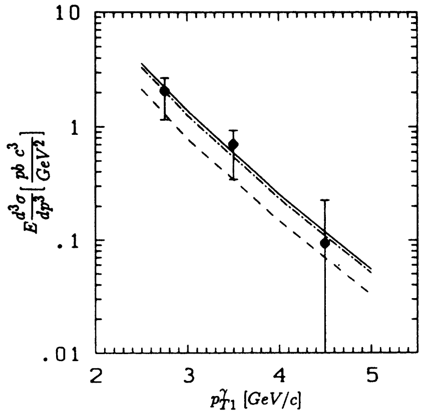


FIG. 15. Invariant cross section for inclusive $\gamma\gamma$ production vs the transverse momentum $p_{T1}^{\gamma}/(\mathbf{p}_{T1}^{\gamma})^2$ of one of the photons. The cross section is integrated over $z=\mathbf{p}_{T1}^{\gamma}\cdot\mathbf{p}_{T2}^{\gamma}/(\mathbf{p}_{T1}^{\gamma})^2$ of the other photon above a value of $z^{\min}=p_{T2}^{\min}/p_{T1}^{\min}$, where $p_{T1}^{\min}$ is the lower edge of the considered bin of the transverse momentum $p_{T1}^{\gamma}$ and $p_{T2}^{\min}$ is 2 GeV/$c$. The dashed curve shows the result of the Born term. The solid curve shows the result of a QCD calculation (Ref. 10) in which all next-to-leading-order processes and the box graph were included, whereas for the dashed-dotted curves bremsstrahlung contributions were excluded.

The good agreement of the experimental and theoretical $\gamma\gamma$ cross section in $\pi^-p$ reactions clearly excludes the renormalizable version of the Han-Nambu model[32] with integrally charged quarks. In this model four of the gluons also acquire integral charges. Mainly because of the gluon contributions this model predicts $\gamma\gamma$ cross sections which are more than an order of magnitude larger than the cross sections obtained by calculations with the usual fractional charge assignment. Because of low statistics no estimation of $\alpha_s$ or intrinsic parton transverse momenta could be obtained.

## V. CONCLUSIONS

When applying isolation criteria around the photons the production of $\gamma\gamma$ events could be observed in $\pi^-p$ re-

TABLE VIII. Upper limits of cross-section ratios (confidence level 90%) for $\gamma\gamma$ production at a c.m.s. energy of $\sqrt{s}=23.7$ GeV. Both photons are required to have a transverse momentum larger than 2 GeV/$c$. For a similar kinematic region the QCD prediction in lowest and next-to-leading order (including the box graph) are listed for comparison.

| | NA24 $p_{T1}^{\gamma},p_{T2}^{\gamma}>2$ GeV/$c$ | Theory $O(\alpha^2)$ | Theory $O(\alpha^2\alpha_s)$ |
|---|---|---|---|
| | | $p_{T1}^{\gamma}=3$ GeV/$c$, $z^{\min}=0.67$ | |
| $\frac{\sigma(\pi^+p\to\gamma\gamma+X)}{\sigma(\pi^-p\to\gamma\gamma+X)}$ | <1.8 | 0.111 | 0.165 |
| $\frac{\sigma(pp\to\gamma\gamma+X)}{\sigma(\pi^-p\to\gamma\gamma+X)}$ | <0.5 | 0.177 | 0.242 |

actions with a statistical significance of $2.9\sigma$. The $\gamma\gamma$ cross section agrees with a higher order QCD calculation.

In the extraction of the $\gamma\gamma$ events also data on $\pi^0\pi^0$ and $\gamma\pi^0$ production were obtained. The invariant double-differential cross section of $\pi^0\pi^0$ production at high $p_T$ was measured. It agrees well with the appropriately scaled results of a Fermilab experiment on $\pi^+\pi^-$ pair production in $p$Be reactions. The validity of a scaling hypothesis of the cross section in $pp$ reactions which was demonstrated by an ISR experiment at the c.m.s. energies $\sqrt{s}=62.4$ GeV and $\sqrt{s}=44.8$ GeV could be extended to the NA24 c.m.s. energy of $\sqrt{s}=23.7$ GeV. In accordance with the expectations of the quark parton model the cross-section ratio $\sigma(\pi^-p\rightarrow\pi^0\pi^0+X)/\sigma(pp\rightarrow\pi^0\pi^0+X)$ is growing both with the mass $M$ and the rapidity $Y$ of the $\pi^0$ pair, whereas the ratio $\sigma(\pi^-p\rightarrow\pi^0\pi^0+X)/\sigma(\pi^+p\rightarrow\pi^0\pi^0+X)$ is consistent with unity.

In $\pi^-p$ and $pp$ reactions a clear signal of $\gamma\pi^0$ events is observed. The invariant $\gamma\pi^0$ cross section is much lower than the single $\gamma$ cross section and falls less steeply with increasing transverse momentum of the photon. In most of the $\gamma\pi^0$ events the photon has a higher transverse momentum than the $\pi^0$.

## ACKNOWLEDGMENTS

We are grateful for excellent technical help provided by R. Ferorelli, H. Fessler, W. Fröchtenicht, B. Gordeev, M. Kellner, M. Mongelli, H. J. Osthoff, M. Perchiazzi, H. Röser, A. Sacchetti, J. Seyboth, and V. Vinogradov. We wish to thank the staff at CERN for the operation of the SPS accelerator and the H2 beam line and the supporting help of the SPS coordinators.

---

*Present address: CERN, Geneva, Switzerland.
†Present address: Bell Labs, Holmdel, New Jersey.
‡Present address: University of Berne, Switzerland.
§Present address: University of Nijmegen, Netherlands.
**On leave of absence from Central Research Institute for Physics, Budapest, Hungary.

[1]C. De Marzo et al., Phys. Rev. D **36**, 8 (1987).
[2]C. De Marzo et al., Phys. Rev. D **36**, 16 (1987).
[3]S. M. Berman et al., Phys. Rev. D **4**, 3388 (1971).
[4]K. Soh et al., Phys. Rev. D **18**, 751 (1980).
[5]M. Krawczyk and W. Ochs, Phys. Lett. **79B**, 119 (1978).
[6]B. L. Combridge, Nucl. Phys. **B174**, 243 (1980).
[7]C. Carimalo et al., Phys. Lett. **98B**, 105 (1981).
[8]S. Hemmi, Prog. Theor. Phys. **63**, 1073 (1980).
[9]E. L. Berger et al., Nucl. Phys. **B239**, 52 (1984).
[10]P. Aurenche et al., Z. Phys. C **29**, 459 (1985).
[11]A. P. Contogouris et al., Phys. Rev. D **35**, 1590 (1987).
[12]C. Kourkoumelis et al., Z. Phys. C **16**, 101 (1982).
[13]J. Badier et al., Phys. Lett. **164B**, 184 (1985).
[14]T. Åkesson et al., Z. Phys. C **32**, 491 (1986).
[15]C. Albajar et al., Phys. Lett. B **209**, 385 (1988).
[16]R. Ansari et al., Z. Phys. C **41**, 395 (1988).
[17]E. Bonvin et al., Z. Phys. C **41**, 591 (1989).
[18]A. Weltin, Diplomarbeit, Freiburg University, 1982 (unpublished).
[19]M. De Palma et al., Nucl. Instrum. Methods **216**, 393 (1983).
[20]V. Artemiev et al., Nucl. Instrum. Methods **224**, 408 (1984).
[21]V. Eckardt et al., Nucl. Instrum. Methods **155**, 389 (1978).
[22]C. De Marzo et al., Nucl. Instrum. Methods **217**, 508 (1983).
[23]G. Donaldson et al., Phys. Lett. **73B**, 375 (1978).
[24]C. Kourkoumelis et al., Nucl. Phys. **B158**, 39 (1979).
[25]C. De Marzo et al., Nucl. Phys. **B211**, 375 (1983).
[26]T. Åkesson et al., Z. Phys. C **25**, 13 (1984).
[27]M. Banner et al., Phys. Lett. **118B**, 203 (1982).
[28]H. Jöstlein et al., Phys. Rev. D **20**, 53 (1979).
[29]A. L. S. Angelis et al., Nucl. Phys. **B209**, 284 (1982).
[30]Original program version, W. Ochs (private communication).
[31]D. W. Duke and J. F. Owens, Phys. Rev. D **30**, 49 (1984); J. F. Owens, ibid. **30**, 943 (1984).
[32]T. Jayaraman, G. Rajasekaran, and S. D. Rindani, Phys. Rev. D **33**, 672 (1986).